NANO LETTERS

2001
Vol. 1, No. 5
227−230

Atomic Scale Imaging by UHV-AFM of Nanosized Gold Particles on Mica

Sylvain Ferrero,* Agnès Piednoir, and Claude R. Henry

CRMC2[†]−CNRS, Campus de Luminy Case 913, 13288 Marseille Cedex 09, France

Received February 21, 2001

ABSTRACT

Gold particles of a mean size of 22 nm are grown epitaxially on a muscovite mica support by atom deposition. For the first time, it is shown that the morphology of nanometer sized gold particles supported on mica can be imaged at the atomic scale in situ by UHV-AFM in contact mode. Top (111) and lateral (100) facets are imaged simultaneously near an edge. On a top (111) facet an atomic step has been observed.

The morphology of metal clusters in heterogeneous catalysts is of key importance to understanding their catalytic activity. However, it is very difficult to get this information on real powder catalysts. On the contrary, flat-model catalysts obtained by growing, under UHV, metal clusters on single crystals (generally oxides) are well suited for basic studies on the mechanisms of heterogeneous catalysis because they can be studied by many surface science techniques.[1] The morphology of the metal particles in flat-model catalysts can be conveniently studied by TEM,[2] but as it is an ex situ technique the air exposure can change the particle morphology. Alternatively, scanning probe microscopy is a suitable tool to study in situ (under UHV or under pressure) the morphology of flat-model catalysts. Scanning tunneling microscopy (STM) is limited to conducting samples. However, instead of a bulk insulating support an ultrathin film (such as Al_2O_3, MgO) supported on a metal single crystal can be used for STM studies.[3] Atomic resolution has been obtained by STM on small Pd clusters supported on graphite or MoS_2[4] and on large Pd clusters supported on alumina thin films on NiAl (110).[5] On bulk insulating supports only AFM can be used. AFM has been already used to study, ex situ in ambient conditions, the morphology of flat-model catalysts.[6−13] However, generally the metal particles appear round due to the convolution with the tip shape. In some cases facets have been observed on large particles such as for Pd on mica[9] and on MgO.[13] In the former case, atomic resolution on the top (111) facets of 20 nm Pd particles has been observed in lateral force.[9] However, from observation in ambient conditions, it is difficult to rule out the possibility of imaging an adsorbed layer. A few papers report on the atomic resolution of metal surfaces by AFM under UHV: one on the Cu(111) surface in lateral force image[14] and one on Ag(111) in noncontact mode.[15] The $23 \times \sqrt{3}$ superstructure of the Au(111) surface has been also imaged in noncontact mode,[16] but no atomic resolution was achieved as in the case of STM.[17]

In this letter we present a UHV-AFM study of gold nanoparticles supported on mica. A detailed study of the morphology and the structure of the gold particles will be presented in a forthcoming paper. Here, we focus on the imaging of the particle facets at atomic scale.

The mica−muscovite (001) substrate was cleaved under nitrogen and immediately transferred in the preparation chamber. The substrate was cleaned under UHV by heating at 500 °C during 5 h, as described by Poppa et al.[18] Gold clusters were epitaxially grown by condensing a calibrated beam of atoms from a Knudsen cell on the mica substrate kept at 450 °C. During the 110 minutes of deposition, the pressure was close to 1×10^{-8} Torr. The typical flux was 2.8×10^{12} cm^{-2} s^{-1}, and the equivalent deposited thickness was about 20 monolayers, as evaluated by a quartz crystal thickness monitor. The heating was switched off just after the deposition, and the sample, after cooling at room temperature, was transferred under UHV in the AFM chamber (2×10^{-10} Torr). All of the observations presented here were performed in contact mode with an OMICRON UHV-AFM.

Figure 1 shows a typical AFM topographic image of the gold deposit on mica. The density of particles is 1.3×10^{11} cm^{-2} and the mean diameter is 22 ± 6 nm. Although the density of particles is large, they are well separated from each other. The highest particles (around 12 nm in height) are the smallest (around 10 nm in diameter). For such size the determination of the actual shape is difficult because of the convolution with the tip shape. Nevertheless, by a comparison between AFM and TEM observations we know that these particles are either tetrahedra, like the one down in the left of the figure (letter A), or multiple twinned

* Corresponding author email: ferrero@crmc2.univ-mrs.fr.

[†] The CRMC2 is associated to the Universities of Aix-Marseille II and III.

10.1021/nl010014i CCC: $20.00
Published on Web 05/09/2001

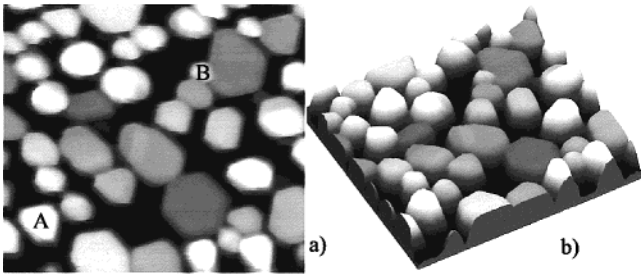

Figure 1. AFM topographic image (200 × 178 nm^2) of gold particles on mica grown at 450 °C. The data were taken with a constant attractive force of 0.4 nN, the gray scale is the *z* scale. (a) 2D top view image, (b) 3D representation. Letters A and B correspond to a tetrahedral and a multiply twinned particle, respectively.

particles with 5-fold symmetry (icosahedra and decahedra) that appear round in AFM images.

The larger particles have a well-defined shape as expected from previous TEM studies:[19] flat hexagons and flat truncated triangles (around 6 nm in height) in epitaxy with the substrate. The edges of these particles are parallel to three directions in respect to the symmetry of muscovite (001) surface. Moreover, electron diffraction showed that the gold particles have a (111) plane in contact with the (001) basal plane of muscovite. Thus, the top facet of a hexagonal or triangular flat cluster should also be a (111) plane. This is demonstrated in Figure 2, which shows three simultaneously recorded images (topographic, lateral force, and normal force images) of the top facet of a flat particle of 30 nm in length. Topographic images correspond to the variation of the tip sample distance. The contrast of the lateral force image and the normal force images correspond to the variation of the lateral force and the normal force, which are given by the torsion and the bending of the cantilever, respectively. The contrast of these last two modes is generally stronger than in the topography image but they cannot give true heights. We can recognize the hexagonal atomic lattice of the Au (111) plane. The mean distance between nearest neighbor bright spots, on topographic or lateral force images, measured from profile lines in a ⟨110⟩ direction (Figure 2b) is 2.86 ± 0.05 Å, which is very close to the lattice distance (2.88 Å) of the Au (111) plane in the bulk. It has been verified that the observed lattice is not due to an experimental artifact as it keeps the same spacing by changing the scanned area or the scan rate. The topographic image gives a corrugation of about 0.3 Å. In the lateral and normal force images, we can see more clearly the three atomic series of rows, corresponding to the three ⟨110⟩ directions. The $23 \times \sqrt{3}$ superstructure of the Au (111) has not been observed, contrary to STM or noncontact AFM results obtained on macroscopic surfaces.[16,17] It is likely that the superstructure has a parameter (6.3 nm) too large to be established on a 20 nm wide facet.

The identification of the lateral facets is necessary to determine the particle morphology. For this purpose, the probe is placed on the top facet of a hexagonal particle (about 30 nm in size), near an edge to image simultaneously both facets. The following AFM images (Figures 3 and 4) are lateral force images on which the lattice resolution is more clearly visible, but all information about heights is taken from topographic images. Figure 3a presents the atomic lattice of a top facet with a thick line showing no clear lattice resolution, which is parallel to the particle edge. The profile (marked by an arrow on Figure 3a) taken perpendicularly to this line on the topographic image recorded simultaneously, reveals a step of 2.4 ± 0.4 Å in height (see Figure 3b). We can reasonably think that it is an atomic step between two (111) planes (the distance between two (111) planes in bulk gold is 2.36 Å). This image shows that it is possible to

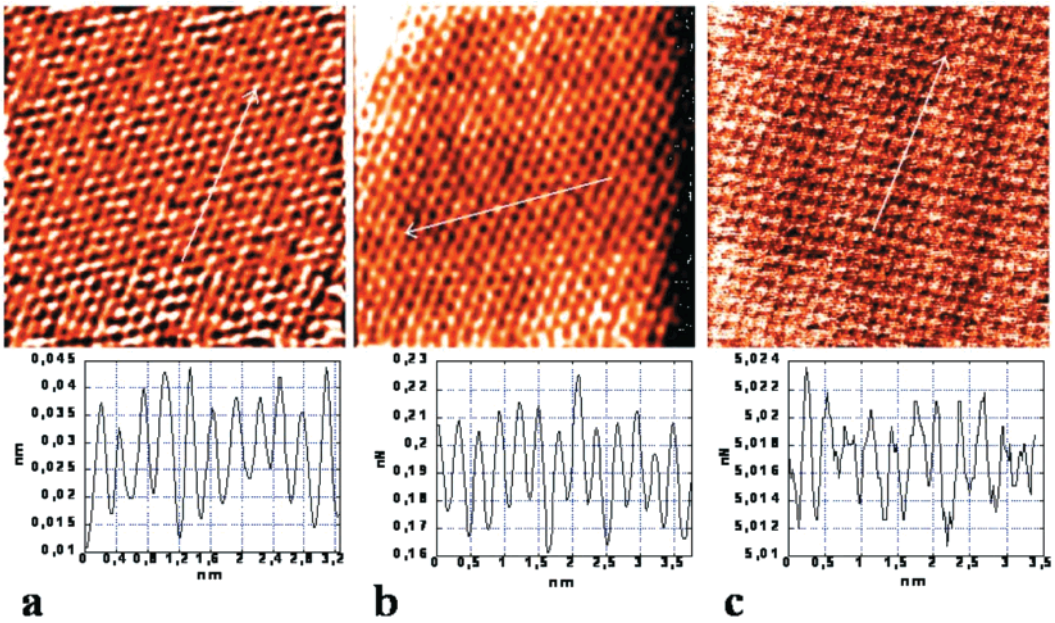

Figure 2. (a) AFM topographic, (b) lateral force, and (c) normal force images (6 × 6 nm^2) of a top facet of a flat gold particle on mica and profiles corresponding to the arrows on the three previous images. The images have been simultaneously recorded in situ (2×10^{-10} Torr) with a constant repulsive force of 5 nN.

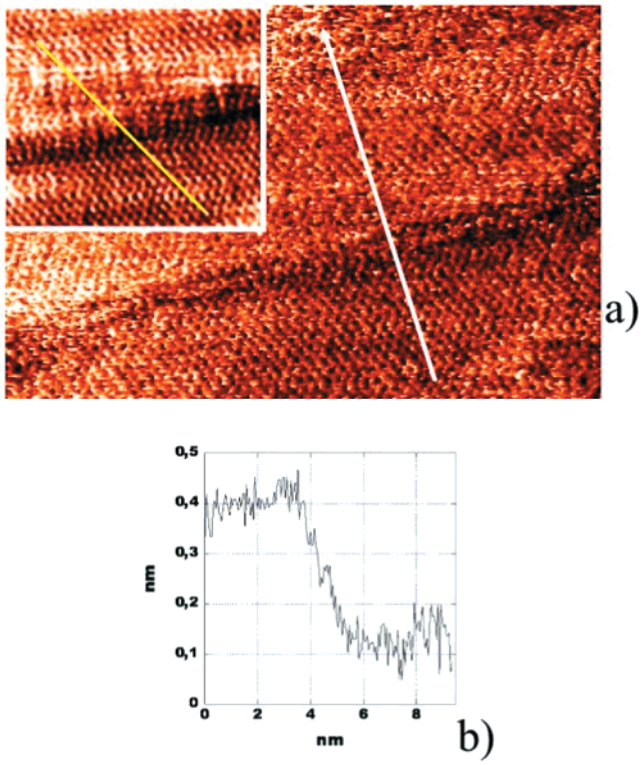

Figure 3. (a) AFM lateral force image (10 nm × 15 nm) of a top facet of a flat gold particle on mica. The data were taken with a constant repulsive force of 5 nN. The inset is an enlargement of the (filtered) image showing the *a*/2 shift of the lattice at the step in the direction indicated by the yellow line. (b) Profile from the topographic image simultaneously recorded, taken perpendicularly to the edge and the step of (2.4 Å in height) as indicated by the white line on the Figure 3a.

observe on lateral force images the atomic lattice of two different terraces separated by a step on which the lattice resolution is lost.

To identify the nature of the lateral facet, the tip has been shifted toward the edge between two facets and the scanned area has been reduced. In Figure 4, one can see the (111) plane of the top facet on the lower half image, limited by an edge separating two facets. Beyond this edge, atomic rows perpendicular to this edge are visible. The Fourier transform of this image confirms the periodicity of the top facet lattice by the presence of four (clearly visible, the two other spots are very faint) of the six spots expected for a (111) plane. In addition, it shows the presence of an atomic lattice by the presence of two additional weak spots, at 30° from the ⟨110⟩ strongest spots. Figure 4b is the back Fourier transform image obtained by selecting the four spots corresponding to two ⟨110⟩ directions of the top facet atomic rows. We see a hexagonal lattice, with a periodicity of 2.8 ± 0.2 Å, corresponding to the lower half of Figure 4a and almost nothing on the upper part. To obtain Figure 4c, the two additional spots have been selected and we clearly see rows only on the upper part of the image (on the other side of the edge) that are perpendicular to the edge with a periodicity of 2.7 ± 0.2 Å. In this way, we can evidence two different atomic lattices separated by an edge.

In the image of Figure 4a we have observed two different atomic lattices: the Au (111) of the top facet, and on the other facet, atomic rows perpendicular to the edge. They are characteristic of an Au (100) facet. Indeed, an Au (100) facet can be described with atomic rows separated by 2.88 Å and that are perpendicular to the edge between the two facets. We can also observe in the lateral force image the loss of lattice resolution near the edge on the (001) facet. It may be explained by the sudden change of slope which causes, as in the case of the atomic step, a decrease of the surface contact between the tip and the sample.

We can explain the better contrast in lateral force imaging by the fact that the tip should be blunt and present a larger interaction area between tip and sample, which will produce a stronger lateral deflection of the cantilever.

According to several authors,[20] it is impossible to obtain true atomic resolution by AFM in contact mode. Indeed, for STM the dependence of tunneling current on the tip-to-sample separation is exponential, and then only the closest atom of the tip interacts with the closest atom of the sample. In AFM, the interaction between tip and sample atoms is weaker, thus several atoms of the apex of the tip interact simultaneously with sample atoms. The resulting image is an average of the contributions given by the apex atoms interacting with the sample. On the contrary, recent molecular

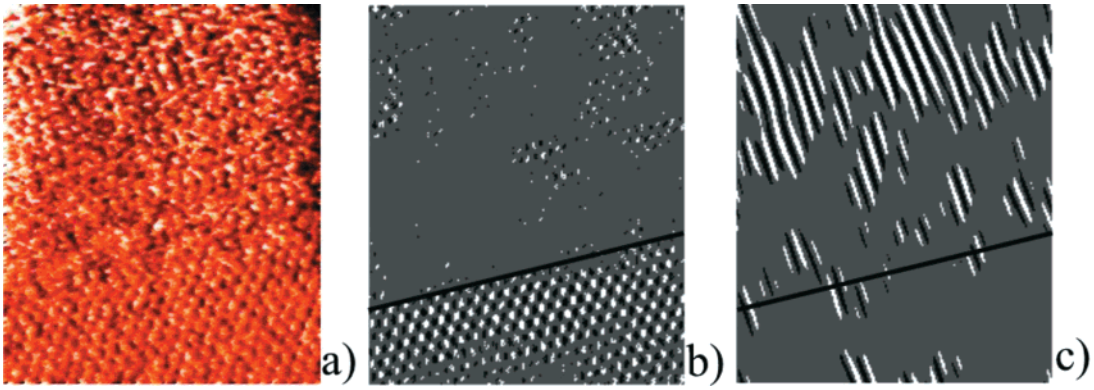

Figure 4. (a) AFM lateral force image (5.7 nm × 6.8 nm) of a top and lateral facets of a flat gold particle on mica. (b) Back Fourier transform of the Fourier transform of the AFM lateral force image (a), selecting only four spots corresponding to the atomic lattice of the top (111) facet. (c) Back Fourier transform of the Fourier transform of the AFM lateral force image (a), selecting only the two spots corresponding to the atomic lattice of the lateral (100) facet.

dynamics simulations have shown that atomic resolution in contact mode is possible on metals.[21] Nevertheless, we have shown that it is possible to visualize two terraces separated by an atomic step. The topographic image gives the height of the step (2.4 ± 0.4 Å) and the lateral force image shows the atomic lattice of the two terraces separated by the step. The line (see inset of Figure 3a) drawn on atomic rows of each terrace shows at the step a shift of $a/2$ expected between the upper and the lower terraces (a is the distance between two neighboring ⟨110⟩ rows). We can see in the lateral force image that the step is characterized by a dark zone (a lower lateral force) of about 2 nm in width. It can be explained by a decrease of the contact area between the tip and the sample when the probe is on top the step leading to a decrease of the lateral force.[22]

We have shown that it is possible to characterize at atomic scale top and lateral facets of nanometer sized metal particles by AFM under UHV in contact mode. We have also imaged linear defects as atomic steps and cluster edges. In the future, we will study, at atomic scale, the evolution of the morphology of metal particles from model catalysts during a chemical reaction.

Acknowledgment. We thank C. Claeys and M. Dayez for technical support.

References

(1) Henry, C. R. *Surf. Sci. Rep.* **1998**, *31*, 231.
(2) Giorgio, S.; Graoui, H.; Chapon, C.; Henry, C. R. In *Metal Clusters in Chemistry*; Braunstein, P., Oro, L. A., Raithby, P. R., Eds.; VCH−Wiley: Chichester, 1999; p 1194.
(3) Bäumer, M.; Freund, H. J. *Prog. Surf. Sci.* **1999**, *61*, 127.
(4) Piednoir, A.; Perrot, E.; Granjeaud, S.; Humbert, A.; Chapon, C.; Henry, C. R. *Surf. Sci.* **1997**, *391*, 19.
(5) Hansen, K. H.; Worren, T.; Stempel, S.; Laegsgaard, E.; Bäumer, M.; Freund, H. J.; Besenbacher, F.; Stensgaard, I. *Phys. Rev. Lett.* **1999**, *83*, 4120.
(6) Colchero, J.; Marti, O.; Mlynek, J.; Humbert, A.; Henry, C. R.; Chapon, C. *J. Vac. Sci. Technol. B* **1991**, *9*, 794.
(7) Erlandsson, R.; Eriksson, M.; Olsson, L.; Helmersson, U.; Lundström, I.; Pettersson, L. G. *J. Vac. Sci. Technol. B* **1991**, *9*, 825.
(8) Mahoney, W.; Schaefer, D. M.; Patil, A.; Andres, R. P.; Reifenberger, R. *Surf. Sci.* **1994**, *316*, 383.
(9) Nie, H. Y.; Shimizu, T.; Tokumoto, H. *J. Vac. Sci. Technol. B* **1994**, *12*, 1843.
(10) Partridge, A.; Toussaint, S. L. G.; Flipse, C. F. J. *Appl. Surf. Sci.* **1996**, *103*, 127.
(11) Fujimoto, T.; Kojima, I. *Appl. Surf. Sci.* **1997**, *121/122*, 257.
(12) Abriou, D.; Gagnot, D.; Jupille, J.; Creuzet, F. *Surf. Rev. Lett.* **1998**, *5*, 387.
(13) Fornander, H.; Birch, J.; Sandström, P.; Sundgren, J. E. *Thin Solid Films* **1999**, *349*, 4.
(14) Bennewitz, R.; Gyalog, T.; Guggisberg, M.; Bammerlin, M.; Meyer, E.; Güntherodt, H. J. *Phys. Rev. B* **1999**, *60*, R11301.
(15) Orisaka, S.; Minobe, T.; Uchihashi, T.; Sugawara, Y.; Morita, S. *Appl. Surf. Sci.* **1999**, *140*, 243.
(16) Molitor, S.; Güthner, P.; Berghaus, T. *Appl. Surf. Sci.* **1999**, *140*, 276.
(17) Barth, J. V.; Brune, H.; Ertl, G.; Behm, R. J. *Phys. Rev. B* **1990**, *42*, 9307.
(18) Poppa, H.; Grant Elliot, A. G. *Surf. Sci.* **1971**, *24*, 149.
(19) Allpress, J. G.; Sanders, J. V. *Surf. Sci.* **1967**, *7*, 1.
(20) See, for example, Shluger, A. L.; Wilson, R. M.; Williams, R. T. *Phys. Rev. B* **1994**, *49*, 4915. Soerensen, M. R.; Jacobsen, K. W.; Stotze, P. *Phys. Rev. B* **1996**, *53*, 2101.
(21) Katagiri, M.; Patrick, D. L.; Lyndenbell, R. M. *Surf. Sci.* **1999**, *431*, 260.
(22) Howald, L.; Haefke, H.; Lüthi, R.; Meyer, E.; Gerth, G.; Rudin, H.; Güntherodt, H. J. *Phys. Rev. B* **1994**, *49*, 5651.

NL010014I